Nanoscale

Helical magnetism in poly(aniline-co-ferrocene): Structure and magnetism

Journal:	*Nanoscale*
Manuscript ID	NR-ART-09-2024-004027.R1
Article Type:	Paper
Date Submitted by the Author:	05-Nov-2024
Complete List of Authors:	Miyashita, Ryo; University of Tsukuba Kawakami, Ryo; University of Tsukuba Kumai, Reiji; High Energy Accelerator Research Organization (KEK) , Institute of Materials Structure Science Tomoita, Takashi; University of Tsukuba Goto, Hiromasa; University of Tsukuba, Institiute of Materials Science

ARTICLE

Helical magnetism in poly(aniline-co-ferrocene): Structure and magnetism

Received 00th January 20xx,
Accepted 00th January 20xx

DOI: 10.1039/x0xx00000x

Ryo Miyashita,[a] Ryo Kawakami,[a] Reiji Kumai [b], Takashi Tomita[a], and Hiromasa Goto*[a]

This study reports the synthesis and characterisation of a ferrocene-based conjugated polymer and a chiral composite. The precursor copolymer was synthesised from 1,3-phenylenediamine and 1,1′-dibromoferrocene via Buchwald–Hartwig polycondensation. This polymerisation process increased the effective conjugation length and led to magnetic spin interactions along the main chain, resulting in a ground triplet spin state at 25°C. Furthermore, the polymer was oxidised with *m*-chloroperoxybenzoic acid and doped with sulfuric acid. A chiral polymer blend was also prepared by combining the copolymer with hydroxypropyl cellulose to form helical polymer liquid crystals. The physical properties of these polymers were analysed using superconducting quantum interference devices, optical spectroscopy, electron spin resonance, and X-ray fluorescence spectroscopy. The resulting polymer blend exhibits helical magnetism. This approach to fabricating a chiral magnetic material from an achiral polymer via supramolecular chirality introduces a new method for preparing chiral magnets.

Introduction

Chirality plays a fundamental role in biology and chemistry, representing broken symmetry in an object, whether in real or reciprocal space. Mirror images of chiral objects cannot be superimposed.[1] Chirality is an indispensable property in living organisms, where different one-handed chiral forms exhibit distinct biochemical and pharmacological properties.[2] For example, the handedness of chiral molecules is crucial for the precise sequences and interactions required for DNA replication, which are vital for the genetic information transfer and for maintaining the structural integrity, stability, and functional efficiency of biological systems. In the field of spintronics, remarkable advancements have been made with inorganic semiconductors through discoveries such as giant magnetoresistance, spin-transfer torque, larger tunnelling magnetoresistance, and spin–orbit torque.[3] These advances have greatly enhanced our understanding and application of spin-based electronics. Notably, when spins moves within a chiral object, they become chiral due to spin–orbit coupling, generating a large spin current in the chiral objects.[4] The spin of a specific one-handed chiral object can move and polarise easily if it aligns with the same handedness; this phenomenon is known as chiral-induced spin selectivity (CISS).[5,6] CISS enables the development of efficient devices that operate at room temperature with low power consumption without relying on heavy elements.[6,7] This phenomenon is also promising for applications in electrochemical asymmetric synthesis[8] and optical resolution using external magnetic fields.[2] Additionally, the spin structure of a chiral magnetic object is described by a chiral alignment called as Skyrmion.[9] Skirmion's topological properties provide stability and low-current drivability, making them suitable for use in high-density, power-efficient memory, and computing devices.[10–12]

Chiral polymers can be prepared by incorporating chiral moieties into side chains or by using supramolecular approaches. Supramolecular chirality arises from chiral aggregation formed via non-covalent interactions, such as hydrogen bonding, π stacking, and van der Waals forces between components.[13] Supramolecular chirality of polyisocyanides with helical rod-like structures allows the formation of 2D hexagonal frame works, applied to immobilize biomolecules with high stability and catalytic activity, and fractionate the size of nanomaterials.[14] Furthermore, supramolecular chirality caused by the co-assembly of achiral luminescent molecules and chiral molecules can produce circularly polarized luminescence (CPL) from the luminescent source without a chiral structure.[15] Self-assembly of helical conjugated polymers exhibits distinct CPL[16,17], and chiral micelles with catalytic moiety such as phosphine can be employed as enantioselective catalysts in asymmetric synthesis and used repeatedly[18]. Our previous work demonstrated that the supramolecular chirality resulting from the combination of a helical liquid crystal (LC) polymer and an achiral conductive polymer leads to a helical arrangement of charge carriers (polarons) responsible for the magnetism and electrical conduction in the conductive polymer.[19]

[a] *Department of Materials Science, Institute of Pure and Applied Sciences, University of Tsukuba, Tsukuba, Ibaraki 305-8573, Japan.*
[b] *Photon Factory, Institute of Materials Structure Science, High Energy Accelerator Research Organization (KEK), Tsukuba, Ibaraki, 305-0801, Japan.*
† Footnotes relating to the title and/or authors should appear here.

Metallocene features a metal atom sandwiched between two cyclopentadienyl rings, with a molecular orbital and electronic configuration resulting from the combination of d- and π-orbitals. Ferrocene, a metallocene with an Fe atom at its centre, was discovered in 1951 and has since found applications in various fields.[20,21] Ferrocene-based molecules are known for their high chemical and thermal stabilities in various environments and versatile synthetic methods.[22] Moreover, metallocene-containing molecules have are of considerable interest for their potential applications in electronic and spintronic devices.[23,24]

Hydroxypropyl cellulose (HPC) is a cellulose derivative characterised by etherified side chains that render it water-soluble. When containing 20%–50% water, HPC exhibits fluidity and birefringence because of its self-organisation into cholesteric liquid crystal.[25,26] Cholesteric LCs form an LC phase through the helical aggregation of LC molecules, exhibiting optical activity. HPC also exhibits good mechanical strength and toughness, making it an important binder for pharmaceutical tablet formulations.[27]

In this study, we report the preparation of a copolymer of 1,3-phenylenediamine (PDA) and 1,1′-dibromoferrocene (DBF) via Buchwald–Hartwig polycondensation, with the aim of preparing a polymer that integrates d- and π-electrons. We compared the interactions of d-electrons with organic radicals and polarons in both the LC state of HPC (helical LC media) and the copolymer to assess the changes in their properties. We evaluated the chemical structures, optical properties, and magnetic properties of these materials. The copolymerisation process expanded the conjugated system, leading to spin interactions along the main chain and forbidden transitions indicative of triplet states, as confirmed by electron spin resonance (ESR) measurements at room temperature. However, in materials doped with sulfuric acid, this forbidden transition could not be observed, likely due to doping-induced carrier generation, which disrupted the conjugated system by introducing holes into the main chain. Furthermore, we prepared an optically active paramagnetic material by blending achiral-conjugated polymers with helical LC.

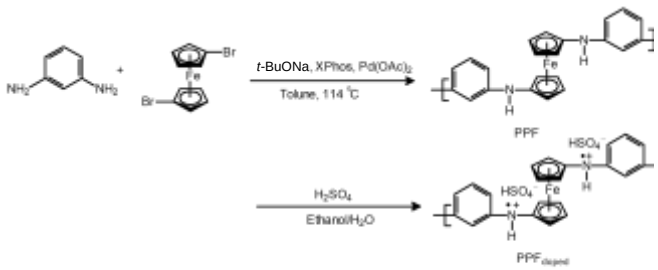

Scheme 1. Synthesis of the copolymer (PPF) and doped form (PPF_{doped}). PDA: 1,3-phenylenediamine. DBF: 1,1′-dibromoferoccene. *t*-BuONa: tert-butoxysodium. $Pd(OAc)_2$: palladium(II) acetate. XPhos: 2-dicyclohexylphosphino-2′,4′,6′-triisopropylbiphenyl.

PPF was oxidised with *m*-chloroperoxybenzoic acid using the Tokumaru method. The reagents—PPF (0.2 g), *m*-chloroperoxybenzoic acid (0.405 g), and chloroform (100 mL)—were stirred overnight at 0°C (Scheme 2). After the reaction, the obtained product was rinsed with a large amount of hexane, filtered, and dried under vacuum. The resultant light brown product was referred to as PPF_{OX}. PPF was doped with sulfuric acid in an ethanol–water solution (Scheme 1). PPF (0.24 g) and sulfuric acid (12 mL) in ethanol (160 mL) and pure water (12 mL) were stirred for 24 h. After the reaction, the resulting product was filtered and dried under vacuum. This product was denoted as PPF_{doped}.

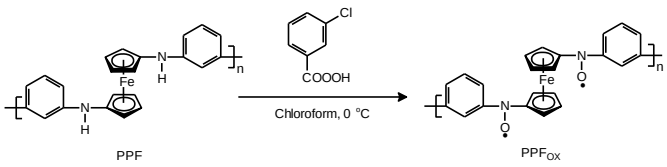

Scheme 2. Synthesis of the PPF with nitroxyl radicals. PPF: copolymer of 1,3-phenylenediamine and 1,1′-dibromoferrocene.

Experimental

Polymer synthesis

PDA was coupled with DBF via Pd-catalysed cross-coupling polycondensation (Buchwald–Hartwig coupling) to yield the copolymer. PDA (0.320 g, 2.960 mmol), DBF (1.000 g, 2.908 mmol), *tert*-butoxysodium (*t*-BuONa, 1.698 g, 17.7 mmol), 2-dicyclohexylphosphino-2′,4′,6′-triisopropylbiphenyl (XPhos, 0.425 g, 0.893 mmol), palladium(II) acetate ($Pd(OAc)_2$, 0.2 g, 0.383 mmol), and toluene (50 mL) were added to a flask and stirred for one day at 114°C under reflux (Scheme 1). The resulting brown product (4.84 g) was washed with hexane. After filtration and vacuum drying, the resultant product was designated as PPF.

Polymer blending

HPC forms lyotropic cholesteric LC exhibiting fluidity and birefringence when mixed with water or *m*-cresol.[25,28] Generally, the main chain of a conjugated polymer synthesised in an isotropic solvent is entangled, a state known as “compact coil.” Dissolving the conjugated polymer in *m*-cresol, a polar solvent, untangles the main chain (expanded coil) improving the crystallinity and conductivity. This procedure is called secondary doping. PPF (0.08 g) and HPC (1.28 g) were stirred in *m*-cresol (0.9 mL) at 10 rpm for four days using a glass rod. The resulting product was dried on a glass slide at room temperature to form films, which are referred to as PPF/HPC. The main chain of PPF formed during helical aggregation by combining secondary doping with *m*-cresol and blending of the helical LC state HPC in *m*-cresol.

Materials

PDA, DBF, *t*-BuONa, and XPhos were purchased from the Tokyo Chemical Industry (TCI, Tokyo, Japan). Toluene was purchased from Nacalai tesque (Kyoto, Japan). *m*-Cresol and *m*-chloroperoxybenzoic acid were purchased from FUJIFILM Wako Pure Chemical Co., Ltd (Osaka, Japan). HPC (viscosity = 2.0–2.9 mPa·s, M_w ≈ 40,000 g/mol) was provided by Nisso (Tokyo, Japan).

Instrument

Polarising optical microscopy (POM) observation was performed using an ECLIPS LV 100 high resolution polarising microscope (Nikon, Tokyo, Japan). Ultraviolet–visible (UV–vis) absorption measurements were carried out using a V-630 spectrophotometer (JASCO, Tokyo). Fourier transform infrared (FT-IR) absorption spectroscopy was performed by FT–IR 4600 (JASCO, Tokyo). Circular dichroism (CD) spectroscopy measurements were carried out using a J-720 spectrometer (JASCO, Tokyo). Scanning electron microscopy (SEM) images were obtained through Tabletop Microscopes TM4000Plus (Hitachi High-Technologies). Electron spin resonance (ESR) spectroscopy measurements were performed on a Japan Electron Optics Laboratory (JEOL, Tokyo) JES TE-200 spectrometer with 100 kHz modulation (X-band). Thermogravimetric, derivative thermogravimetric, differential thermal analysis were performed using DG/DTA 7300 (Seiko Instruments Inc.) Synchrotron X-ray diffraction measurements were conducted at a BL-8B line in synchrotron KEK. Magnetic properties were evaluated using a superconductor quantum-interference device (SQUID, Quantum Design CA, magnetic property measurement system, MPMS). The results of Raman spectroscopy were obtained by NRS–5100 (JASCO, Tokyo). X-ray fluorescence spectroscopy results were acquired via Microscopic X–Ray Fluorescent Analyzer SEA 5210A (Hitachi High-Technologies). The molecular weight of the polymer was investigated by gel permission chromatography via a Shodex A-80 M column and a JASCO HPLC 870-UV detector with THF used as solvent with the instrument calibrated by polystyrene standard.

Results and discussion

Infrared absorption, Raman spectroscopy, and gel permission chromatography

DBF, PDA, PPF, PPF_{OX}, PPF_{doped}, and PPF/HPC were identified via Fourier transform infrared (FT-IR) spectroscopy using the KBr method. Figs. 1a and 1b present the FTIR spectra for DBF, PDA, PPF, PPF_{OX}, PPF_{doped}, and PPF/HPC ranging from 4000 to 400 cm^{-1} and 4000 to 2000 cm^{-1}, respectively. The absorption bands at 1013 cm^{-1} in PPF_{OX} and 991 cm^{-1} of PPF_{doped} are attributed to C–H in-plane bending in the CP of DBF.[29] However, the corresponding band in the PPF was not observed because it overlapped with PDA absorption band. Furthermore, the band corresponding to DBF and PDA in PPF/HPC was difficult to confirm due to the overlap with the OH signals of HPC in the range of 1600–1500 cm^{-1}. Two split absorption bands corresponding to NH_2 stretching were observed at 3397 and 3332 cm^{-1} in PDA.[30] Additionally, a broad absorption band due to NH stretching was observed in PPF, PPF_{OX}, PPF_{doped}, and PPF/HPC[31,32] at 3443, 3448, 3442, and 3448 cm^{-1}, respectively, indicating the formation of DBF and PDA copolymers. Absorptions corresponding to quinonoid (Q) structures were confirmed at 1600, 1554, and 1634 cm^{-1} in PPF, PPF_{OX}, and PPF_{doped}, respectively. Meanwhile, the peak corresponding to the benzenoid (B) were only observed at 1437 and 1428 cm^{-1} in PPF and PPF_{OX}, respectively. Generally, the main chains of aromatic conjugated polymers are connected by benzenoid structures, which have lower energy than Q structures. The transition to a Q structure is caused by electron depletion (withdrawal). Therefore, PPF_{doped} exhibited a Q signal. PPF/HPC dipicted an absorption due to CH_2 and CH_3 stretching of HPC at 2974 cm^{-1}. Table 1 lists the FTIR spectral assignments of DBF, PDA, PPF, PPF_{OX}, PPF_{doped}, and PPF/HPC.

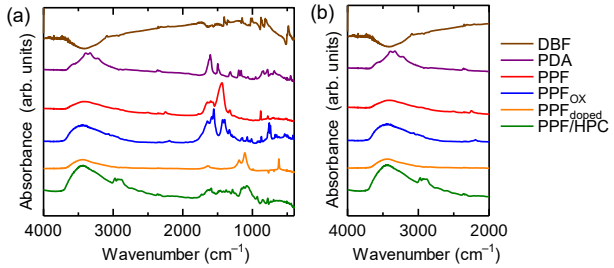

Fig. 1. Fourier transform infrared spectra for DBF, PDA, PPF, PPF_{OX}, PPF_{doped}, and PPF/HPC: (a) full scale in the range of 4000–400 cm^{-1}, selected scales in the range of (b) 4000–2000 cm^{-1}. PDA: 1,3-phenylenediamine. DBF: 1,1'-dibromoferoccene. PPF: The copolymer of PDA and DBF. PPF_{OX}: The oxidised PPF with *m*-chloroperoxybenzoic. PPF_{doped}: PPF doped with sulfuric acid. PPF/HPC: The composite with PPF and hydroxypropyl cellulose (HPC).

Table 1. Assignment of FTIR spectra of DBF, PDA, PPF, PPF_{OX}, PPF_{doped}, and PPF/HPC. PDA: 1,3-phenylenediamine. DBF: 1,1'-dibromoferoccene. PPF: The copolymer of PDA and DBF. PPF_{OX}: The oxidised PPF with *m*-chloroperoxybenzoic. PPF_{doped}: PPF doped with sulfuric acid. PPF/HPC: The composite with PPF and hydroxypropyl cellulose (HPC).

	$\nu_{NH,NH2}$	ν_{OH}	ν_{BQB}	ν_{B}	$\delta_{C-H(CP)}$ in-plane bending
DBF	—[1]	—[1]	—[1]	—[1]	1005
PDA	3332 3397	—[1]	—[1]	—[1]	—[1]
PPF	3443	—[1]	1600	1437	—[2]
PPF_{OX}	3448	—[1]	1554	1428	1013
PPF_{doped}	3442	—[1]	1634	—[1]	991
PPF/HPC	3448	2974	—[2]	—[2]	—[2]

[1] No signal. [2]Overlap.

Fig. 2 shows the Raman spectroscopy measurement of DBF, PDA, and PPF in the range of 4000–400 cm^{-1} The two

absorption bands at 1405 and 1377 cm^{-1} in DBF are attributed to C=C stretching in CP.[33] Absorption corresponding to NH_2 and C–N vibration were observed[34] at 1600 and 1316 cm^{-1}, respectively. In PPF, two absorption bands corresponding to C=C stretching in CP were observed at 1508 and 1461 cm^{-1}. Additionally, an absorption band due to the Q structure was observed at 1554 cm^{-1}, while no absorption corresponding to NH_2 was confirmed. The results of FTIR and Raman spectroscopy measurements indicate that a copolymer of DBF and PDA was successfully obtained using the method described in this study.

Gel permission chromatography measurement for PPF was carried out using tetrahydrofuran (THF) as the eluent with standard poly(styrene) calibration to evaluate the molecular weight. The number- average molecular weight (M_n) and the weight-average molecular weight (M_w) of PPF were 5,525 and 24,304; respectively. Furthermore, the molecular weight distribution (M_w/ M_n) was 4.40. Notably, the soluble fraction of PPF was measured because of the insolubility and infusibility, and the molecular weight determined by the measurement is lower than the total fractions of PPF.

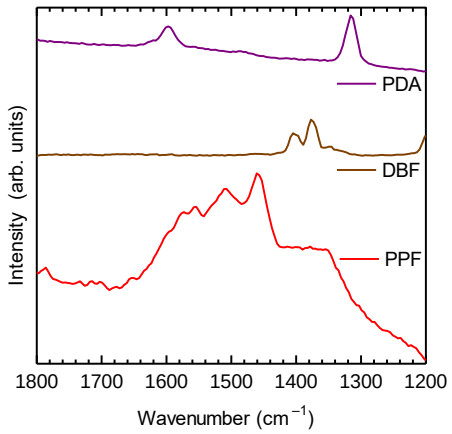

Fig. 2. Raman spectra for PDA, DBF, and PPF. PDA: 1,3-phenylenediamine. DBF: 1,1′-dibromoferoccene. PDA: 1,3-phenylenediamine. DBF: 1,1′-dibromoferoccene. PPF: The copolymer of PDA and DBF.

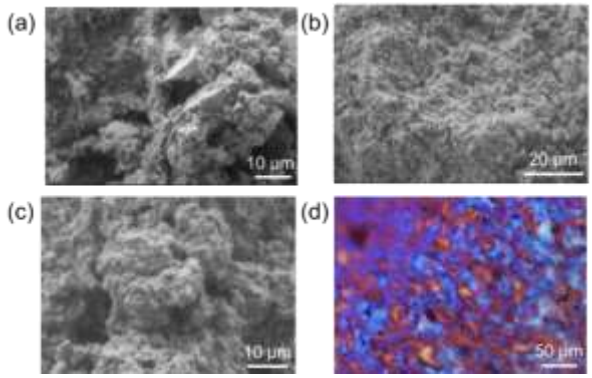

Fig. 3. Scanning electron microscopy images of (a) PPF, (b) PPF_{OX},, and (c) PPF_{doped}. (d) Polarising optical microscopy image of PPF/HPC with the insertion of a gypsum first-order red plate. PPF: The copolymer of 1,3-phenylenediamine and 1,1′-dibromoferrocene. PPF_{OX}: The oxidised PPF with *m*-chloroperoxybenzoic. PPF_{doped}: PPF doped with sulfuric acid. PPF/HPC: The composite with PPF and hydroxypropyl cellulose (HPC).

Surface observation and thermal analysis

PPF, PPF_{OX}, and PPF_{doped} were observed using scanning electron microscopy (SEM). Figs. 3a–c display SEM images of these materials, which reveal heterogeneous porous cotton-like polymer structures. Fig. 3d shows a polarising optical microscopy image of PPF/HPC with the insertion of a gypsum first-order red plate, indicating birefringence. The birefringence is derived from the helical LC state of HPC. In the blending of PPF with the helical LC state of HPC, PPF was finely mixed within the HPC matrix.

Thermogravimetry (TG), derivative TG (DTG), and differential thermal analysis (DTA) measurements of the PPFs were conducted under an Ar flow. Fig. 4a shows the TG and DTG curves for PPF, and Fig. 4b shows the DTA measurement results for PPF. The thermal degradation and DTG peaks of PPF under 150°C were attributed to the evaporation of residual solvent.[35] The DTA peak corresponding to endothermic processes resulting from solvent evaporation was observed at 96°C. Furthermore, DTG peaks associated with thermal degradation were confirmed at 300°C, 363°C, and 472°C.[36] The mass loss of PPF was approximately 23%, and PPF was stable up to 500°C.[37]

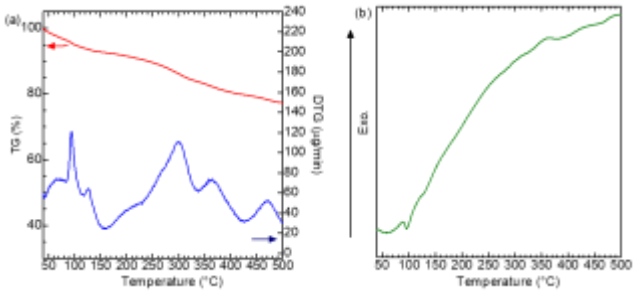

Fig. 4. (a) Thermogravimetric (TG, red line) and derivative thermogravimetric (DTG, blue line) curves for PPF. (b) Differential thermal analysis curve for PPF. PPF: copolymer of 1,3-phenylenediamine and 1,1′-dibromoferrocene.

Electrical conductivity and X-ray fluorescence spectroscopy

The electrical conductivities of PPF and PPF_{doped} were measured using the four-point probe method. The electrical conductivity of PPF was low (1.44×10^{-7} S/cm). The conduction is possibly involved electron hopping.[22] However, PPF_{doped} showed no conductivity ($<1 \times 10^{-9}$ S/cm). Generally, aromatic conjugated polymers showed conductivity after doping with counter ions, such as I^-, SO_4^-, and ClO_4^-. Specifically, conjugated polymers with benzene aromatic rings, such as polyaniline, form a continuous chain of Q structures, allowing the delocalization of polarons along the main chain and enabling electrical conduction. In contrast, the meta-linked polymer showed no electrical conductivity because the Q structure could not form a continuous linkage along the main chain, resulting in localised polarons. The presence of Fe atoms in PPF and PPF_{doped} was confirmed via X-ray fluorescence (XRF) spectroscopy. Figs. 5a and 5b show the XRF spectroscopy results for PPF and PPF_{doped}, respectively. Fluorescence photon peaks corresponding to the K_α and K_β lines of the Fe were observed at 6.40 and 7.1 eV in PPF.[38–40] Similarly, the fluorescence photon peaks were confirmed at 6.40 and 7.06 eV in PPF_{doped}.

ESR spectroscopy measurements were conducted for DBF, PPF, PPF_{OX}, PPF_{doped}, and PPF/HPC. Figs. 6a and 6b show the ESR signals of PPF in the range of 305–330 mT and 130–175 mT (half-field), respectively. Figs. 6c and 6d show the ESR signals of PPF_{OX} in the range of 300–360 mT and 120–190 mT (half-field), respectively. Fig. 6e shows the ESR signal of PPF_{doped} in the range of 325–334 mT. The condition for ESR is described by the following equation:

$$\Delta E = h\nu = g\beta H \qquad (1)$$

where β is the Bohr magneton, H is the resonance magnetic field, h is the Planck's constant, g is a material-specific value determined by the electron spin environment, and ν is the resonance frequency. DBF exhibited a broad ESR signal (peak-to-peak width: 46.9 mT) at g = 2.2, which is attributed to the electrons of the Fe atoms.[41] However, the signal associated with the forbidden transition of $\Delta M_s = \pm 2$, indicating a ground triplet spin state,[42–44] was not observed at g ≈ 4.0. In contrast, PPF exhibited a signal at g = 2.00294, corresponding to radicals on the main chain due to structural defects. The signal from an Fe atom could not be confirmed, likely because it overlapped with the signal from radicals on the main chain.

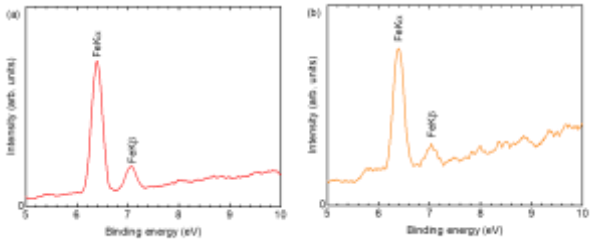

Fig. 5. X-ray fluorescence spectroscopy results for (a) PPF and (b) PPF_{doped}. PPF: The copolymer of 1,3-phenylenediamine and 1,1′-dibromoferrocene. PPF_{doped}: PPF doped with sulfuric acid.

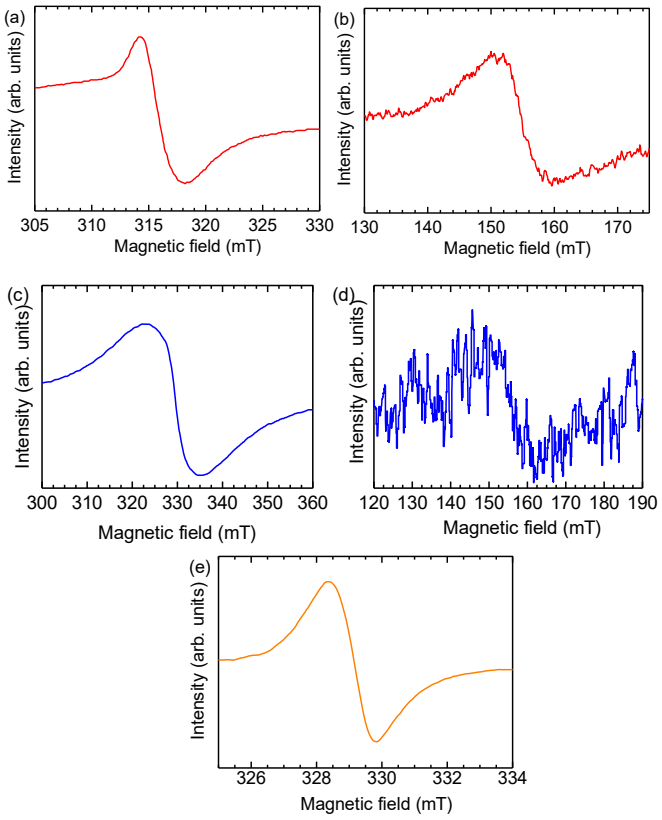

Fig. 6. Electron spin resonance (ESR) spectra of PPF: (a) 305–330 mT and (b) 130–175 mT. ESR spectra of PPF_{OX}: (c) 300–360 mT and (d) 120–190 mT. (e) ESR spectrum of PPF_{doped} at 325–334 mT. PPF: The copolymer of 1,3-phenylenediamine and 1,1′-dibromoferrocene. PPF_{OX}: The oxidised PPF with *m*-chloroperoxybenzoic. PPF_{doped}: PPF doped with sulfuric acid.

Furthermore, a signal at g ≈ 4.0, ranging from 130 to 175 mT at 25°C was observed, which is derived from the forbidden transition, confirming that PPF is in a ground triplet state. This forbidden transition is caused by the interaction between ferrocene molecules via π-orbitals due to the longer conjugation lengths from copolymerisation.[45] PPF_{OX} exhibited an ESR signal at g = 2.0071, caused by nitroxyl radicals,[46] which overlapped with the signal from Fe electrons. Moreover, PPF_{OX} showed a signal at g ≈ 4.0 at 25°C, confirming the forbidden transition and the ground triplet state, despite the generation of nitroxyl radicals on the main chain. The ESR signal of PPF_{doped} at g = 2.0047 corresponded to the polaron of the polymer, overlapping with the Fe electron signal. However, the signal associated with the forbidden transition was not observed. Normally, *p*-linked conjugated polymers such as *p*-PANI exhibit electrical conduction in the doped state due to

the delocalization of polarons, the carriers for electrical conduction, enabled by the linkage of Q structures on the main chain (Fig. 7a). In contrast, *m*-linked conjugated polymers such as PPF_{doped} forms no continuous Q structure linkage, resulting no electrical conductivity. In particular, *m*-PANI doped with sulfuric acid is believed to lack a conjugated structure in the ring, leading to localisation of carriers on the main chain (Fig. 7b). This plausible structure was simulated using density functional theory calculations in a *m*-linked aniline oligomer as an example, yielding the lowest energy structure (Fig. 7c). Thus, PPF_{doped} is deficient in the conjugated structure spreading along the main chain due to sulfuric acid doping, which explains the absence of a forbidden transition signal in the ESR spectra. Additionally, this could account for the lack of electrical conductivity. The ESR signals of PPF/HPC were no observed, likely due to dielectric relaxation caused by residual *m*–cresol.

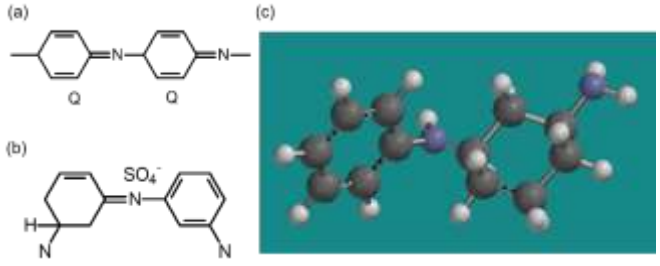

Fig. 7. (a) Linkage of quinonoid (Q) structures on the main chain of *p*-PANI. (b) Plausible linkage of Q structures in *m*-PANI. (c) Theoretical structure of the Q linkage in *m*-PANI simulated using density functional theory calculation.

Optical properties and plausible structure

The optical absorption properties of DBF, PDA, PPF, PPF_{OX}, PPF_{doped}, and PPF/HPC in the solid state were evaluated via ultraviolet-visible (UV–vis) spectroscopy (Fig. 8a). UV–vis measurements of DBF, PDA, PPF, PPF_{OX}, and PPF_{doped} were performed in 1-methyl-2-pyrrolidone (NMP) solution (all materials were dispersed at a concentration of 0.4 g/L). As a monomer, PDA exhibited no absorption band above 320 nm. In contrast, DBF, as a monomer, exhibited an absorption maximum of 435 nm. PPF, PPF_{OX}, and, PPF_{doped} exhibited multiple optical absorptions from 320 to 500 nm, corresponding to π–π* transition of the main chain caused by the increase in the conjugate length during polymerisation. Furthermore, PPF/HPC exhibited a wide absorption band from 320 nm to ca. 800 nm. PPF/HPC is a composite material formed by mixing PPF with *m*–cresol to entangle the main chains, thereby mixing it with HPC/*m*-cresol, a polymer lyotropic LC. The polymer blend method increases the effective conjugated chain length of the main chain by secondary doping with polar solvents and using LC molecules as a template, resulting in PPF/HPC with broad optical absorption. Fig. 8b shows the circular dichroism (CD) absorption spectra of PPF in NMP (PPF was disperesed at a concentration of 0.4 g/L) solution and PPF/HPC in the solid state. PPF exhibits no CD absorption at short to long wavelengths. In contrast, PPF/HPC exhibits negative CD absorption at 360–580 nm, which corresponds to its optical activity. The optical activity was attributed to the helical aggregation of the main chain, which was introduced by blending HPC as the helical LC.

Synchrotron radiation X-ray diffraction (XRD) (λ = 0.997 Å) measurements for PPF and PPF/HPC were conducted on the BL-8B beamline of the Photon Factory at the High Energy Accelerator Research Organization. Figs. 8c and 8d show the circle-type diffraction patterns of PPF and PPF/HPC with synchrotron XRD. Fig. 8e shows the diffraction signals of PPF and PPF/HPC. PPF has no characteristic peaks in 2θ range of 7°–20°. Additionally, a broad signal corresponding to a slightly ordered amorphous phase of HPC was observed at 4.6 Å for PPF/HPC.[47] Molecular aggregation of PPF in HPC, a cholesteric LC, forms the main chain in a one-handed helical conformation. In other words, polymer blending with the cholesteric polymer LC induces a helical main chain in the conjugated polymer. Fig. 9 shows the possible helical aggregation morphology of PPF in HPC.

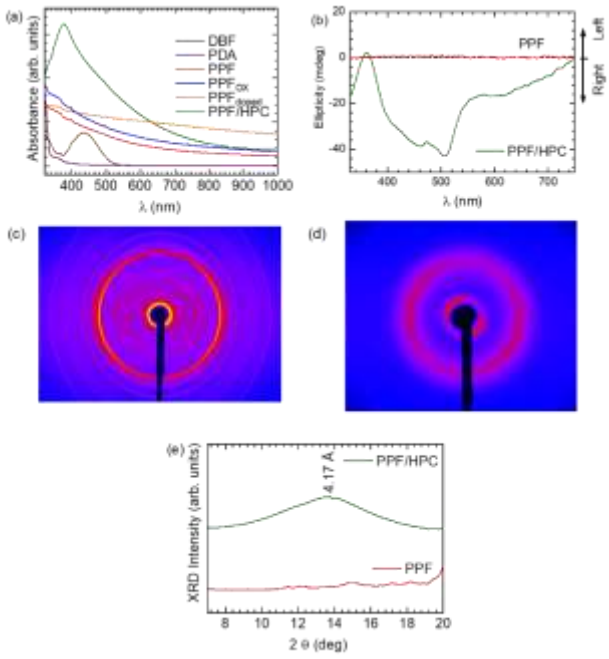

Fig. 8. (a) Ultraviolet–visible absorption spectra of DBF, PDA, PPF, PPF_{OX}, PPF_{doped}, and PPF/HPC. (b) Circular dichroism optical absorption spectra of PPF and PPF/HPC. Diffraction pattern of (c) PPF and (d) PPF_{doped}. (e) X-ray diffraction profiles of PPF and PPF_{doped} in the range of 7°–20°. PDA: 1,3-phenylenediamine. DBF: 1,1'-dibromoferoccene. PPF: The copolymer of PDA and DBF.

PPF_{OX}: The oxidised PPF with *m*-chloroperoxybenzoic. PPF_{doped}: PPF doped with sulfuric acid. PPF/HPC: The composite with PPF and hydroxypropyl cellulose (HPC).

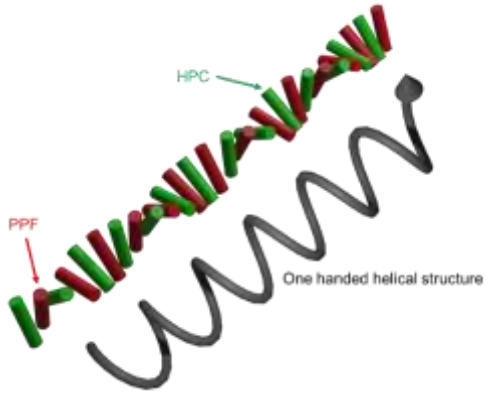

Fig. 9. Possible helical aggregation morphology of PPF in HPC. PPF: The copolymer of 1,3-phenylenediamine and 1,1′-dibromoferrocene. HPC: hydroxypropyl cellulose.

Magnetic properties

Fig. 10a shows the temperature dependences of the magnetic susceptibilities (χ) for PPF, PPF_{OX}, PPF_{doped}, and PPF/HPC measured using a SQUID in an applied field of 1000 Oe. The χ of all polymers increased with decreasing temperature, implying paramagnetic. PPF_{OX} with two magnetic species, nitroxyl radical and Fe atoms of the ferrocene unit, exhibited the largest χ value per weight. PPF_{doped} exhibited a weaker χ than PPF and PPF_{OX} due to a defect in the conjugated system caused by doping with sulfuric acid. Furthermore, the χ value per weight of PPF/HPC was the smallest because of the composite, which reduced the number of magnetic species of PPF per weight. Fig. 10b–e depicts the temperature dependences of the inverse susceptibility for PPF, PPF_{OX}, PPF_{doped}, and PPF/HPC. The extrapolated θ temperature of PPF (−1.6 K) was higher than that of PPF_{OX} (−2.9 K) even though the χ value of PPF was lower than that of PPF_{OX}. This result indicates that PPF_{OX} has increased magnetic susceptibility due to the increased number of magnetic species, but it has no influence on magnetic interactions. The θ of PPF_{doped} was −4.8 K, which is lower than that of PPF. This phenomenon arises from defects in the conjugated system and weak magnetic interactions. Furthermore, the θ temperature of PPF/HPC was −9.2 K, which is the lowest among the polymers because HPC inhibits the interaction between the PPF main chains via helical aggregation during composite formation. Fig. 10f shows the external field dependences of χ for PPF and PPF/HPC at 4 K. The χ of PPF increased with the magnetic field, indicating a typical paramagnetic behaviour. However, PPF/HPC exhibits a maximum χ value at ≈10000 Oe and is repulsive to high external magnetic fields. The results indicate that the magnetic property of PPF/HPC is a mixture of paramagnetic and diamagnetic behaviour.[48–50] The position of the spins in the main chain is helical and the dipole field produced by the spins in PPF/HPC is asymmetric. In other words, the magnetic structure forms helical shape[51]. The helical magnets behave paramagnetically and antiferromagnetically[52,53]. As the blend system, the overall magnetism of PPF/HPC exhibited helical magnetism. Spin cancellation caused by the helical spin configuration and the strong repulsion of the diamagnetism of atom, molecule, and ion, and Landau diamagnetism[54] against the external magnetic field with an increase in the external magnetic field could be responsible for the diamagnetic property at higher magnetic fields. The copolymer arranged in a helical manner with a guide of the host HPC exhibited helical magnetism. These results suggest that PPF/HPC is an opt-functional magnetic material prepared from an achiral-conjugated polymer by blending polymer LC.

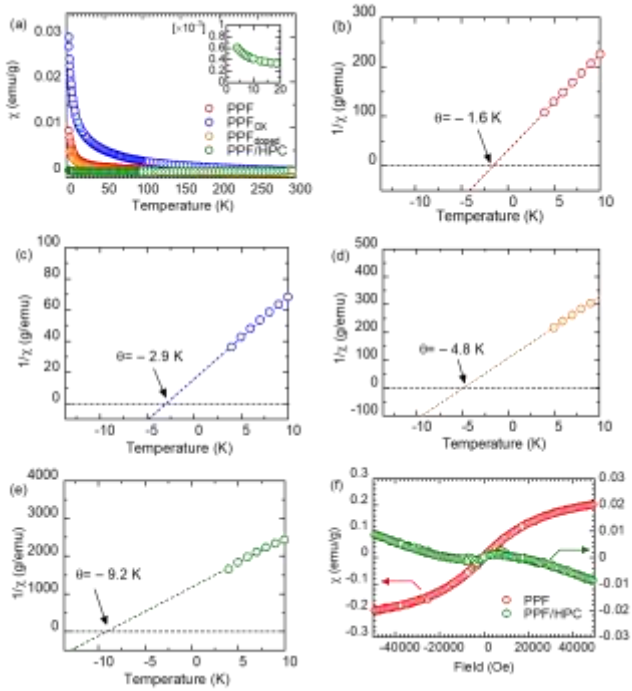

Fig. 10. Superconductor quantum interference device measurement results. (a) χ vs. *T* for PPF, PPF_{OX}, PPF_{doped}, and PPF/HPC. (b) 1/χ vs. *T* of PPF. (c) 1/χ vs. *T* of PPF_{OX}. (d) 1/χ vs. *T* of PPF_{doped}. (e) 1/χ vs. *T* of PPF/HPC. (f) χ vs. magnetic field (*H*) of PPF and PPF/HPC. PPF: copolymer of 1,3-phenylenediamine and 1,1′-dibromoferrocene. PPF_{OX}: oxidised PPF with *m*-chloroperoxybenzoic. PPF_{doped}: PPF doped with sulfuric acid. PPF/HPC: composite with PPF and hydroxypropyl cellulose (HPC).

Conclusions

A conjugated polymer combining π- and d-electrons was successfully prepared using Pd-catalysed cross-coupling polycondensation. ESR measurements at 25°C revealed signals indicative of a ground triplet spin state, characterised by spin alignment. Additionally, the polymer blend method,

incorporating a LC with a helical structure, resulted in a polymer exhibiting helical magnetism and optical activity. This study demonstrates that supramolecular chirality can be harnessed to develop unique chiral magnetic materials through composite formation.

Author contributions

Ryo Miyashita: methodology, formal analysis, investigation, data curation, visualization, writing–original draft, writing–review & editing. Ryo Kawakami: methodology. Reiji Kumai: methodology. Hiromasa Goto: investigation, conceptualization, funding acquisition, methodology, project administration, supervision, writing–review & editing. All authors have read and agreed to the published version of the manuscript.

Conflicts of interest

There are no conflicts to declare.

Data availability

The data that support the findings of this study are available from the corresponding author upon reasonable request.

Acknowledgments

We would like to thank the OPEN FACILITY, Research Facility Centre for Science and Technology, University of Tsukuba. This research was supported by the Japan Society for the Promotion of Science under Grants-in-Aid for Scientific Research (No. 23K04848) and JST SPRING, Japan Grant Number JPMJSP2124. Synchrotron XRD measurements were conducted at the KEK (Photon Factory Program Advisory Committee, Proposal No. 2023G520, H. Goto).

ORCID

Hiromasa Goto: 0000-0003-4276-735X

Ryo Miyashita: 0009-0002-2225-192X

Reiji Kumai: 0000-0002-5320-0028

Notes and references

1 M. Zhang, M. Kim, W. Choi, J. Choi, D. H. Kim, Y. Liu and Z. Lin, *Prog. Polym. Sci.*, 2024, **151**, 101800.
2 K. Banerjee-Ghosh, O. Ben Dor, F. Tassinari, E. Capua, S. Yochelis, A. Capua, S.-H. Yang, S. S. P. Parkin, S. Sarkar, L. Kronik, L. T. Baczewski, R. Naaman and Y. Paltiel, *Science*, 2018, **360**, 1331–1334.
3 S.-H. Yang, *Appl. Phys. Lett.*, 2020, **116**, 120502.
4 S.-H. Yang, R. Naaman, Y. Paltiel and S. S. P. Parkin, *Nat. Rev. Phys.*, 2021, **3**, 328–343.
5 R. Naaman, Y. Paltiel and D. H. Waldeck, *Nat. Rev. Chem.*, 2019, **3**, 250–260.
6 Z. Xie, T. Z. Markus, S. R. Cohen, Z. Vager, R. Gutierrez and R. Naaman, *Nano Lett.*, 2011, **11**, 4652–4655.
7 M. Suda, Y. Thathong, V. Promarak, H. Kojima, M. Nakamura, T. Shiraogawa, M. Ehara and H. M. Yamamoto, *Nat. Commun.*, 2019, **10**, 2455.
8 T. S. Metzger, S. Mishra, B. P. Bloom, N. Goren, A. Neubauer, G. Shmul, J. Wei, S. Yochelis, F. Tassinari, C. Fontanesi, D. H. Waldeck, Y. Paltiel and R. Naaman, *Angew. Chem. Int. Ed.*, 2020, **59**, 1653–1658.
9 C. Pfleiderer, T. Adams, A. Bauer, W. Biberacher, B. Binz, F. Birkelbach, P. Böni, C. Franz, R. Georgii, M. Janoschek, F. Jonietz, T. Keller, R. Ritz, S. Mühlbauer, W. Münzer, A. Neubauer, B. Pedersen and A. Rosch, *J. Phys. Condens. Matter*, 2010, **22**, 164207.
10 C. Back, V. Cros, H. Ebert, K. Everschor-Sitte, A. Fert, M. Garst, T. Ma, S. Mankovsky, T. L. Monchesky, M. Mostovoy, N. Nagaosa, S. S. P. Parkin, C. Pfleiderer, N. Reyren, A. Rosch, Y. Taguchi, Y. Tokura, K. von Bergmann and J. Zang, *J. Phys. Appl. Phys.*, 2020, **53**, 363001.
11 A. Fert, V. Cros and J. Sampaio, *Nat. Nanotechnol.*, 2013, **8**, 152–156.
12 J. Wencong, L. Chen, K. Zhou, L. Li, Q. Fu, Y. Du and R. Liu, *Appl. Phys. Lett.*, 2019, **115**, 192403.
13 M. Liu, L. Zhang and T. Wang, *Chem. Rev.*, 2015, **115**, 7304–7397.
14 R. Gao, S. Li, Y. Zong, Z. Chen, N. Liu and Z. Wu, *Angew. Chem.*, 2024, **136**, e202410010.
15 B.-H. Liu, Y. Zong, N. Liu and Z.-Q. Wu, *Sci. China Chem.*, 2024, **67**, 3247–3257.
16 R.-T. Gao, S.-Y. Li, B.-H. Liu, Z. Chen, N. Liu, L. Zhou and Z.-Q. Wu, *Chem. Sci.*, 2024, **15**, 2946–2953.
17 N. Liu, R.-T. Gao and Z.-Q. Wu, *Acc. Chem. Res.*, 2023, **56**, 2954–2967.
18 L. Xu, L. Zhou, Y.-X. Li, R.-T. Gao, Z. Chen, N. Liu and Z.-Q. Wu, *Nat. Commun.*, 2023, **14**, 7287.
19 R. Miyashita and H. Goto, *ACS Appl. Polym. Mater.*, 2022, **4**, 796–805.
20 U. Rauf, G. Shabir, S. Bukhari, F. Albericio and A. Saeed, *Molecules*, 2023, **28**, 5765.
21 K. Heinze and H. Lang, *Organometallics*, 2013, **32**, 5623–5625.
22 C. Engtrakul and L. R. Sita, *Nano Lett.*, 2001, **1**, 541–549.
23 R. Liu, S.-H. Ke, H. U. Baranger and W. Yang, *Nano Lett.*, 2005, **5**, 1959–1962.
24 R. Liu, S.-H. Ke, W. Yang and H. U. Baranger, *J. Chem. Phys.*, 2007, **127**, 141104.
25 R. S. Werbowyj and D. G. Gray, *Mol. Cryst. Liq. Cryst.*, 1976, **34**, 97–103.
26 D. V. Saraiva, R. Chagas, B. M. de Abreu, C. N. Gouveia, P. E. S. Silva, M. H. Godinho and S. N. Fernandes, *Crystals*, 2020, **10**, 122.
27 L. Cheng, Z. Mo, Q. Zhang, M. Yang, X. Liao, L. Qiu, S. Wang, X. Yang and X. Hu, *J. Chromatogr. A*, 2023, **1711**, 464452.
28 H. Yousefi, G. Wiberg, M.-L. Skytt, J. J. Magda and U. W. Gedde, *Polymer*, 2003, **44**, 1203–1210.
29 P. A. Silva, T. M. R. Maria, C. M. Nunes, M. E. S. Eusébio and R. Fausto, *J. Mol. Struct.*, 2014, **1078**, 90–105.
30 J. B. Peri, *J. Phys. Chem.*, 1966, **70**, 2937–2945.
31 G. Salman, *Polym. Bull.*, 2023, **80**, 9343–9351.
32 N. Wang, C. Zhao, G. Long, B. Xia, L. Wan, K. Niu, J. Hou, J. Wang, L. Lei and Z. Wang, *Materials*, 2023, **16**, 1478.

33 G. F. S. Andrade, L. J. A. Siqueira, M. C. C. Ribeiro, O. Sala and M. L. A. Temperini, *J. Raman Spectrosc.*, 2006, **37**, 498–507.
34 H. M. Badawi, W. Förner and S. A. Ali, *Spectrochim. Acta. A. Mol. Biomol. Spectrosc.*, 2013, **112**, 388–396.
35 B. Vijaya, M. U. Rani and R. S. Babu, *Mater. Res. Express*, 2023, **10**, 055303.
36 J. L. de la Fuente, M. Ruiz-Bermejo, C. Menor-Salván and S. Osuna-Esteban, *Polym. Degrad. Stab.*, 2011, **96**, 943–948.
37 K. Sashmitha and M. U. Rani, *J. Mater. Sci. Mater. Electron.*, 2023, **34**, 850.
38 K. Geraki, M. J. Farquharson and D. A. Bradley, *Phys. Med. Biol.*, 2002, **47**, 2327–2339.
39 P. D. Barman, A. K. Maurya, S. Ghosh, A. Roy and M. Madaan, *Spectrochim. Acta Part B At. Spectrosc.*, 2024, **211**, 106823.
40 V. M. Chubarov, A. A. Amosova and A. L. Finkelshtein, *Inorg. Mater.*, 2020, **56**, 1423–1430.
41 V. V. Zelentsov, Yu. V. Yablokov, M. A. Augustyniak-Jabłokow, A. Krupska, J. Mroziński and V. A. Ulanov, *Chem. Phys.*, 2004, **301**, 15–26.
42 G. P. Moharana, S. K. Singh and H. K. Narayanan, *J. Magn. Magn. Mater.*, 2021, **527**, 167707.
43 A. Nagata, S. Hiraoka, S. Suzuki, M. Kozaki, D. Shiomi, K. Sato, T. Takui, R. Tanaka and K. Okada, *Chem. – Eur. J.*, 2020, **26**, 3166–3172.
44 S. S. Eaton, K. M. More, B. M. Sawant and G. R. Eaton, *J. Am. Chem. Soc.*, 1983, **105**, 6560–6567.
45 Y. Morisaki and Y. Chujo, *Macromolecules*, 2003, **36**, 9319–9324.
46 K. Nakahara, S. Iwasa, J. Iriyama, Y. Morioka, M. Suguro, M. Satoh and E. J. Cairns, *Electrochimica Acta*, 2006, **52**, 921–927.
47 A. H. Basta, V. F. Lotfy, J. A. Micky and A. M. Salem, *Carbohydr. Polym. Technol. Appl.*, 2021, **2**, 100103.
48 L.-C. Tien and Y.-Y. Hsieh, *Mater. Res. Bull.*, 2014, **60**, 690–694.
49 X. Mao, Y. Xu, Q. Xue, W. Wang and D. Gao, *Nanoscale Res. Lett.*, 2013, **8**, 430.
50 A. S. Ganeshraja, S. Thirumurugan, K. Rajkumar, K. Zhu, Y. Wang, K. Anbalagan and J. Wang, *RSC Adv.*, 2016, **6**, 409–421.
51 J. Kishine, K. Inoue and Y. Yoshida, *Prog. Theor. Phys. Suppl.*, 2005, **159**, 82–95.
52 D. C. Johnston, *Phys. Rev. B*, 2017, **96**, 104405.
53 H. Higashikawa, K. Okuda, J. Kishine, N. Masuhara and K. Inoue, *Chem. Lett.*, 2007, **36**, 1022–1023.
54 K. Komaba, H. Yoneyama and H. Goto, *ACS Appl. Polym. Mater.*, 2024, **6**, 2504–2512.

Helical antiferromagnetism in poly(aniline-co-ferrocene): Structure and magnetism

By Ryo Miyashita, Ryo Kawakami, Reiji Kuma, Hiromasa Goto

The data that support the findings of this study are available from the corresponding author, H. G., upon reasonable request.